Journal of Fluorescence, Vol. 11, No. 3, September 2001 (© 2001)

Fluorescence Methods to Probe Nanometer-Scale Organization of Molecules in Living Cell Membranes

R. V. Krishnan,[1,2] R. Varma,[1,2] and S. Mayor[1,3]

The ability to study the structure and function of cell membranes and membrane components is fundamental to understanding cellular processes. This requires the use of methods which are capable of resolving structures at nanometer-scale resolution in living cells. In this review we survey fluorescence imaging methodologies capable of nanometer-scale resolution. We then critically examine specific biological applications of these methods, in the context of understanding membrane protein conformation and dynamics, intracellular signaling, organization of lipid rafts, and cell surface topology.

KEY WORDS: Fluorescence microscopy; digital imaging; FRET; TIR-FM; NSOM; signaling; membrane protein; lipid rafts.

INTRODUCTION

Our understanding of the structural and functional organization of living cell membranes has increased tremendously due to the development of various biophysical tools to look at submicron length scales in living cells. It is increasingly clear that no single experimental technique will cover the entire range of length scales with equal sensitivity and resolution, hence a number of techniques are often used to study structure and function at different biologically relevant length scales (Fig. 1). Conventional light microscopy is sufficient to probe intercellular interactions in an ensemble of cells like those in the environment of the extracellular matrix. However, to study the organization of a few protein or lipid molecules, techniques that will probe the nanometer scale are necessary. Realization of the need to probe submicron- or nanometer-scale organization of membrane components is the premise of this review.

Although electron microscopy offers a spatial resolution of the order of a few nanometers, it cannot be used for examining living specimens due to the demands of working in a vacuum chamber with appropriately fixed specimens [1]. Fluorescence microscopy, on the other hand, offers a noninvasive means to probe various physiological processes in living cells and tissues with relatively high spatial and temporal resolution [2]. This has been made possible due primarily to the development and use of nonperturbing fluorescent probes, capable of being conjugated to biomolecules [3–5]. The ability to image the intrinsic fluorescence of biomolecules such as the green fluorescent protein (GFP) [6], phycobiliproteins [7], or other endogenous small molecules such as serotonin [8] has also greatly facilitated our understanding of the organization of the components in cell membranes of living systems.

In this review, we outline different fluorescence imaging methods available to study submicron-level organization of membrane components and their interactions and provide examples for their applications in bio-

[1] Cellular Organization and Signaling Group, National Centre for Biological Sciences, UAS-GKVK Campus, Bellary Road, Bangalore 560 065, India.
[2] These authors contributed equally to this review.
[3] To whom correspondence should be addressed. E-mail: mayor@ncbs.res.in

1053-0509/01/0900-0211$19.50/0

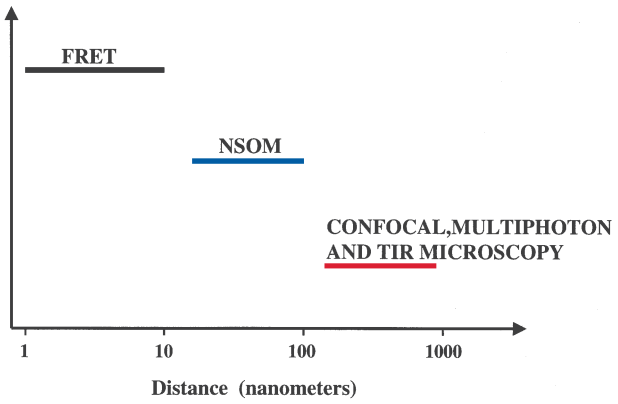

Fig. 1. The resolution limit in various microscopy methods.

logical systems, and finally, we conclude with a brief mention of future perspectives.

FLUORESCENCE IMAGING METHODS

The spatial resolution (r) of a light (or fluorescence) microscope is given by the Rayleigh criterion which is a function of the wavelength (λ) of light and numerical aperture (N.A.) of the lens

$$r = 0.61\lambda/(\text{N.A}) \quad (1)$$

Thus, the resolution of conventional fluorescence microscopes as well as the modern state of the art confocal microscope (single- and multiphoton excitation) in two dimensions is limited: ~250 nm for 550-nm excitation light and a 1.4-N.A. objective lens [9]. Compared to wide-field microscopes, confocal systems have an added advantage, offering higher axial (z-axis) resolution (~500 nm) by eliminating out-of-focus contributions, allowing three-dimensional (3D) reconstruction of fluorescent images. This has allowed micron-scale resolution in imaging of the distribution of molecules in 3D in living cells [2]. However, various physiological and metabolic processes in cells result from interaction between macromolecules on the length scales of a few nanometers. To probe these interactions, it becomes necessary to extend the resolution limit to the nanometer scale.

Extensions of fluorescence microscopy resolution are based on utilizing the physical properties of fluorescence emission [e.g., fluorescence resonance energy transfer (FRET)] [10] or optical innovations in improving the resolution of the excitation source such as near-field scanning optical microscopy (NSOM) [11,12], and total internal reflection fluorescence microscopy (TIR-FM) [13,14]. Figure 1 provides a relative scale of the resolution limit obtained using a variety of techniques.

Fluorescence Resonance Energy Transfer (FRET) Methodology

FRET is a quantum mechanical property of a fluorophore resulting in nonradiative energy transfer between the excited state of the donor fluorophore and a suitable acceptor fluorophore via dipole–dipole interactions. The energy transfer efficiency depends on the relative orientation and separation between the two transition dipoles as well as on the overlap between the donor emission and the acceptor absorption spectra. Figure 2 schematically illustrates the orientational relationships and spectral overlaps between the donor–acceptor pair in the FRET process. More importantly, the transfer efficiency varies inversely as the sixth power of the distance between the

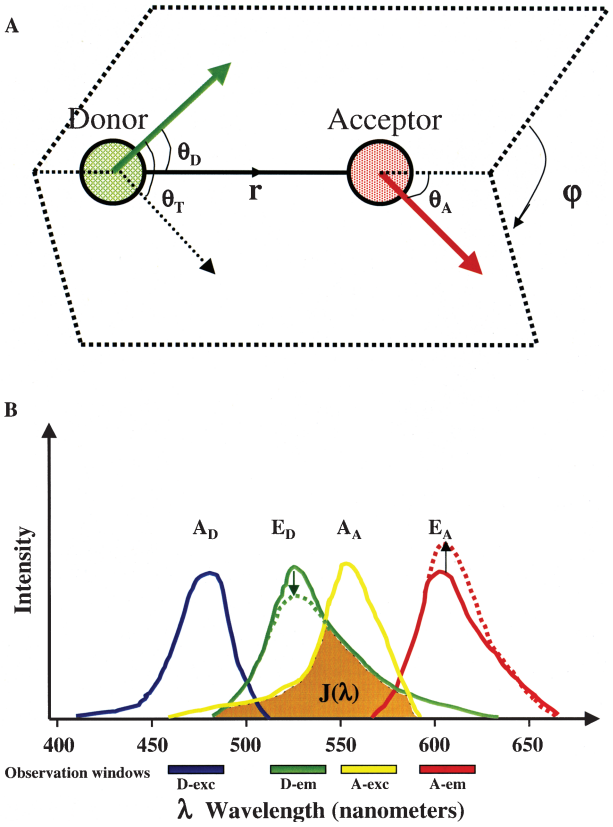

Fig. 2. Schematic depiction of the fluorescence resonance energy transfer process. (**A**) Orientation of donor and acceptor transition dipoles. The relative angle between the two transition dipoles is responsible for the depolarization of fluorescence upon energy transfer. (**B**) Overlap integral $J(\lambda)$between the donor emission (E_D) and the acceptor absorption spectra (A_A). A_D and E_A are the donor absorption and acceptor emission spectra, respectively. Arrows depict the decrease in donor emission and increase in acceptor emission intensities upon energy transfer. Observation windows show excitation and emission wavelength bandwidths for a typical imaging experiment, indicating the potential for cross-talk between the different imaging channels. D, donor; A, acceptor, exc, excitation; em, emission.

donor and the acceptor, thereby serving the purpose of the oft-quoted *spectroscopic ruler* in molecular interactions [15]. The energy transfer efficiency is given by

$$E = [1/\{1 + (r/R_o)^6\}] \quad (2)$$

where r is the distance of separation between the donor and the acceptor fluorophore. R_o ("Forster distance") is defined as that separation for which the energy transfer efficiency is 50% and is calculated using the following expression:

$$R_o = 8.79 \cdot 10^{-5} [n^{-4} \cdot Q \cdot \kappa^2 \cdot J(\lambda)]^{1/6} \text{ Å} \quad (3)$$

where n is the refractive index of medium in the range of overlap, Q is the quantum yield of the donor in the absence of acceptor; and $J(\lambda)$ is the spectral overlap as shown in Fig. 2B. κ^2 is the *orientation* factor, which depends on the relative orientation of the two dipoles (Fig. 2A) and is defined by

$$\kappa^2 = [\cos\theta_T - 3\cos\theta_A \cdot \cos\theta_D] \quad (4)$$

In general, this orientation factor can vary from 0 to 4 but is usually assumed to be 2/3, a value corresponding to a random orientation of the donors and acceptors. Unless explicitly determined by measurements of fluorescence anisotropy [16], it is often erroneous to assume a value for κ^2, since this may result in significant errors in the measurement of distances [17]. However, in some biological situations it may not make a great deal of difference [18]. Typically, R_o varies between 1 and 10 nm for various pairs of fluorophores [15].

There are several consequences of this energy transfer event, namely, (i) quenching of donor fluorescence (Fig. 2B), (ii) sensitized emission of the acceptor (Fig. 2B), (iii) a reduction in the donor lifetime, (iv) an increase in the donor fluorescence emission anisotropy, and (v) depolarization of the sensitized acceptor emission. The design of a FRET experiment depends on which of the consequences is being monitored [10,19].

In the simplest situation, the extent of donor quenching may be taken as a good measure of FRET efficiency and this can be calculated from the relative fluorescence yield in the presence (F_{AD}) and in the absence (F_D) of the acceptor.

$$E = 1 - (F_{AD}/F_D) \quad (5)$$

For imaging purposes, this translates into collecting an image of donor fluorescence and a separate image of acceptor fluorescence. The ratio of donor fluorescence to acceptor fluorescence is then compared to the ratio of donor fluorescence to acceptor fluorescence collected under conditions where there is no likelihood of FRET between donor and acceptor. The use of ratio imaging is particularly important since this will take care of local variations of donor and acceptor fluorescence [20,21]. The extent of donor quenching may be quantified for an entire cell or a given region of a cell at light resolution. One of the drawbacks of this approach is that both donor and acceptor fluorescences are prone to quenching by the environment of the cell or the subcellular organelle where this phenomenon is being observed, leading to erroneous results.

Another experimental design to measure FRET exploits the property of donor dequenching upon acceptor photobleaching. First established by Jovin *et al.* [19] and further extended by Edidin and co-workers [22,23], this is a very useful technique, as it directly yields energy transfer efficiencies and is generally unaffected by environmental factors. Images of cells labeled with a particular ratio of donor and acceptor are taken. Then the acceptor is bleached using either a laser or an arc lamp and another image of the donor, postbleaching, is collected. Care should be taken to establish that the acceptor is completely bleached and there is no phototoxicity of this bleaching reaction. The extent of increase in donor fluorescence postbleaching is used to calculate the energy transfer efficiencies given by Eq. (5), where F_{AD} is the fluorescence yield of the donor in the presence of and F_D is that after photobleaching of the acceptor. Important considerations to be kept in mind are that the acceptor should be sufficiently photolabile and the light source should have a uniform light intensity output during the time of collecting the donor fluorescence image pre- and postbleaching. One way of overcoming the light intensity variation is by normalizing the signal with respect to the light intensity. This is quite easily achieved in a confocal microscope. A donor fluorescence image is collected and then the acceptor may be selectively bleached within a smaller region of the field using the zoom function. Images of donor and acceptor fluorescence are then collected from the entire field, and the donor fluorescence from cells wherein the acceptor has been bleached is normalized to neighboring cells where the acceptor has not been bleached (Fig. 3). The time required to bleach most acceptors can be quite long using conventional wide-field illumination sources (5–7 min [19,24]), and hence these measurements cannot monitor events in real time, unless one has a very photolabile acceptor and high-power laser sources which do not cause photodamage to the tissues.

A frequently used means of detecting FRET is to observe the sensitized emission of the acceptor [10, 25]. However, the efficiency of FRET is difficult to estimate; the reader is referred to Ref. 25 for a detailed account of

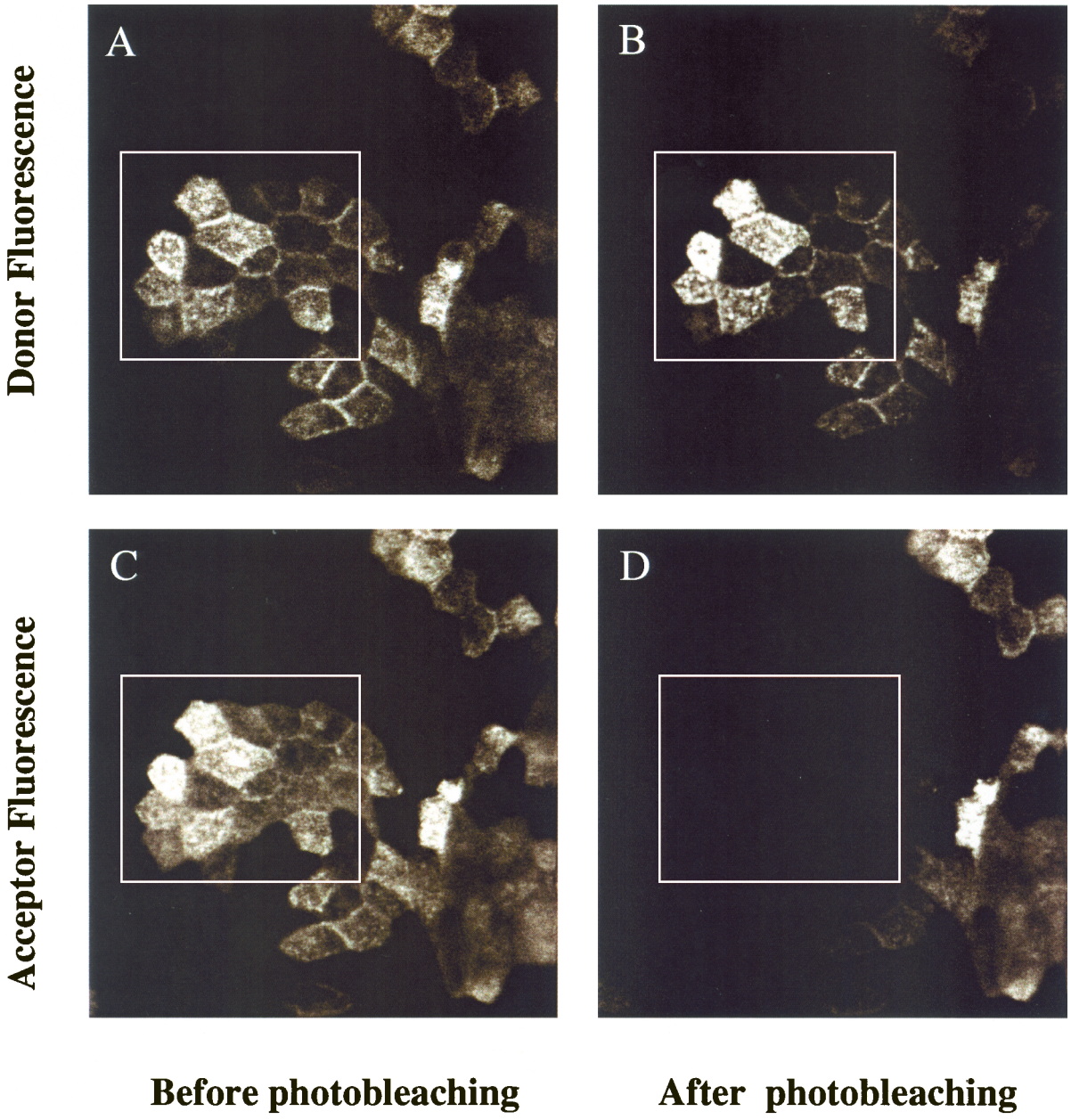

Fig. 3. Implementation of acceptor photobleaching methodology on the confocal microscope. Fluorescence images of a donor (Alexa-568-labeled-Mov18; A, B) in the presence of an acceptor (Cy5-labeled-Mov19; C, D) bound to folate receptors at the surface of Chinese hamster ovary (CHO) cells, pre (A, C)- and post (B, D)-bleaching of acceptors within the indicated square. Note that only cells wherein acceptor fluorophores are bleached (compare C and D) show enhanced donor fluorescence (compare the donor fluorescence in A and B within the same square). For quantitative purposes, the average ratio of donor fluorescence pre- and postbleaching is calculated for all the cells within the square and normalized to the ratio obtained for the cells outside the square. This normalization results in elimination of fluctuations in illumination intensity or other factors during the long photobleaching period. Mov 18 and Mov 19 are monoclonal antibodies to the GPI-anchored folate receptor which recognize different epitopes on the receptor and hence are capable of binding the same receptor.

this calculation. Despite this drawback, the above method has provided one of the first examples of FRET microscopy in living cells (see Table I in Ref. 19). Though very straightforward in concept (Fig. 2B) and easy to implement, this experimental paradigm has a lot of practical problems when used for imaging FRET. The choice of the excitation and emission wavelength bandwidths is critical. This is because the sensitized emission signal

collected is a composite of fluorescence due to the direct excitation of the acceptor at the donor excitation wavelength, spillover fluorescence from the donor into the acceptor fluorescence channel, autofluorescence, and, finally, a contribution from the sensitized emission signal (Fig. 2B). Corrections of "cross-talk" can become very difficult and, if not done appropriately, may mask the energy transfer signal completely [25]. Removal of autofluorescence from the signal is also difficult. Nagy *et al.* have recently described the use of multispectral imaging to correct for the contribution of autofluorescence [26], and using GFP as a special case, Billington and Knight have extensively discussed techniques for distinguishing specific fluorescence from autofluorescence [27]. A general rule of thumb is that the energy transfer signal should be at least above 10–15% of the total signal observed in the acceptor channel and be relatively free of cellular autofluorescence. The development of new donor (e.g., lanthanides [28]) and acceptor (e.g., Cy5 [29]) fluorophores allows temporal and/or spectral distinction between sensitized emission and other contaminating signals. Temporal separation of the lanthanide fluorescence from other signals has been described recently and is relatively easy to achieve, since lanthanides have a millisecond lifetime compared to most fluorophores, which have a nanosecond lifetime [30]. This is especially useful because sensitized emission from lanthanides as donor fluorophores may be collected long after the direct excitation acceptor emission has decayed [28].

A consequence of FRET between spectrally distinct donors and acceptors is that the fluorescence lifetime of the donor species is reduced. The energy transfer efficiency (E) may also be directly calculated from the fluorescence lifetime of the donor in the presence (τ_{AD}) or absence (τ_D) of the acceptor as

$$E = 1 - (\tau_{AD}/\tau_D) \tag{6}$$

This may be directly measured via a recently evolving and powerful methodology called fluorescence lifetime imaging microscopy (FLIM) [31,32]. There are two methods of measuring fluorescence lifetimes; a time domain method and a frequency domain method. In the time domain, fluorescence decays are directly measured after exciting with a short pulse of light [31]. In the frequency domain, the sample is excited with a light wave whose intensity is oscillating sinusoidally at a range of frequencies in the region of the reciprocal of the lifetime that is being measured. The fluorescence intensity emitted will also be sinusoidally varying in intensity at the same frequency but will have a different phase and amplitude. The changes in phase and amplitude are used to calculate the phase τ_φ and modulation τ_M lifetimes. These lifetimes are the same if the sample comprises only a single fluorescent species but will differ in samples that are heterogeneous or in which the single fluorescent species exhibits more than one exponential decay [32]. The main advantage of the FLIM technique is that the FRET signal depends only on the excited rate reactions and not on the donor concentration or light path length. However, this method requires a more involved instrumentation.

An indirect consequence of the change in excited-state lifetimes is a reduction in the number of donor fluorophores in the excited state. This reduces the rate of photobleaching of the donor species, specifically in the presence of the acceptor species. This is a phenomenon exploited by a method pioneered by Jovin *et al.* called photobleaching FRET (pbFRET), wherein the photobleaching rate of the donor is measured. Application of this methodology to FRET imaging has been described extensively in a previous publication [19]. However, it also involves the collection of multiple images to calculate the rates of photobleaching over a relatively long period of time [19,33].

Our laboratory has developed a different methodology for performing FRET microscopy, termed D-FRET [34]. This method utilizes another well-known consequence of FRET, namely, concentration-dependent depolarization of fluorescence [35]. When donor fluorophores are excited with plane polarized light and their rotational diffusion times are longer than the lifetime of the fluorophores, they emit fluorescence which is relatively polarized [36]. However, if they transfer energy to neighboring acceptors, due to the large allowed angular spread for this transition [Eq. (4); see also Fig. 2A], there is an extensive depolarization of the sensitized emission from the acceptor. This method is also capable of monitoring homotransfers between like fluorophores, since FRET will cause a net decrease in emission anisotropy [37,38]. The efficiency of FRET in this case is given simply by

$$E = 1 - (r/r^0) \tag{7}$$

where r and r^0 are the anisotropy (a measure of fluorescence polarization) of donor fluorescence in the presence and absence of FRET conditions for the homotransfer event, respectively. Equation (7) is valid only under the simplest situations, where the sole reason for the change in anisotropy may be attributable to nonradiative transfer to other donor species, where excitation after leaving the donor never returns to the same donor species, and where there is no change in the donor lifetimes [37].

Instrumentation required for these measurements can be easily implemented in a conventional microscope with the proper placement and alignment of excitation and

emission polarizers [34]. Since fluorescence anisotropy is an intrinsic property of fluorescence emission, it is independent of the light path and other environmental effects that affect fluorescence intensity measurements. A requirement of the D-FRET method is that the donor fluorophore must have a nonzero value of anisotropy to begin with, and the neighboring "acceptor" species must have a relatively random orientation and/or some rotational freedom to register sufficient depolarization of fluorescence emission [38]. Fluorescence emission anisotropy is also sensitive to the viscosity of the environment and the mass attached to the fluorescent probe [36], since these factors affect the rotational rates. In practice, the determination of the actual transfer efficiencies by this method may be complicated by several factors [37].

This method is particularly advantageous while probing organizations such as small clusters at membrane surfaces or in solution. When a single fluorophore is used for labeling, every molecule is capable of being both donor and acceptor, thus the probability of FRET between molecules in a small cluster is very high [38]. A large variety of fluorophores should be capable of undergoing D-FRET, thereby allowing the measurement of D-FRET and Forster's radii under different conditions. GFP has recently been shown to be a suitable probe for D-FRET (Sharma *et al.*, manuscript in preparation [39,40]), providing a useful tool to study the organization of many GFP-tagged proteins inside cells at nanometer-scale resolution. In addition, this methodology may be used to study the interaction of two or more proteins (see Fig. 4). It should also be possible to implement these measurements in a confocal arrangement, allowing visualization of nanometer-scale interactions between proteins in intracellular compartments [40]. It should be noted that anisotropy of fluorescence emission is sensitive to the mode of excitation; single- and multiphoton excitation may result in different anisotropy values [41].

Excitation Resolution Enhancement

Another means of increasing the resolution is to reduce the extent of spread of illumination intensity at the excitation side by exploiting the wave properties of light near a surface. These methods have resulted in two types of microscopy, namely, total internal reflection fluorescence microscopy (TIR-FM) and near-field scanning optical microscopy (NSOM).

In TIR-FM, an imaging methodology pioneered by Axelrod and co-workers (reviewed in Ref. 14), an electromagnetic wave is incident at the critical angle (or greater) on an interface between two media of differing refractive indices so that the wave is totally internally reflected into the medium with a higher refractive index (Fig. 5). In biological applications, this interface can be that between the cell and its substrate or that between the cell surface and water. This surface-specific evanescent wave has a well-characterized penetration depth—typically of the order of $\lambda/10$ to λ—and an exponentially decaying intensity that depends on the relative refractive index and incident angle [14]. This method, therefore, provides a way to excite selectively fluorescent molecules located at the interface of two regions having different refractive indices. Fluorescence emission is detected by conventional optics. A major advantage of this method is that it may be implemented with simple instrumentation that includes high-NA objectives and a suitably positioned laser source in an ordinary inverted epifluorescence microscope [14]. An alternative approach is to use a prism instead of the objective lens to provide a TIR excitation as pioneered by Axelrod and co-workers [42] (see Fig. 5). One drawback of this method is that while it enhances resolution in the *z* direction, it is limited by light resolution in the *x*–*y* plane, albeit with very low out-of-focus contributions from fluorophores situated at large distances from the reflecting surface.

NSOM combines scanning probe imaging and near-field fluorescence excitation [12,43]. The heart of an NSOM system is the narrow aperture, usually the sharpened tip of an optical fiber, which serves as a light source for subwavelength illumination and a scanning system similar to that of an atomic force microscope (AFM). When an electromagnetic wave emerges from this narrow aperture, it is confined to the near field (10–100 nm) of the aperture. Among several approaches that have been adopted for producing subwavelength illumination, one successful approach has been to use a metal-coated glass micropipette with an inner diameter of less than 50 nm. An important feature of NSOM is that it couples both enhanced spatial resolution of probing microscopies and measurement of topographic and optical signals [44]. Disadvantages of this method are poor light throughput from the restricted aperture, the instrumentation required to operate a near-field scanning stage or probe, and the difficulty in manufacturing reliable scanning tips reproducibly [45]. Furthermore, applications to imaging in living cells have been limited, possibly due to the inherent difficulty involved [43].

Recently Klar *et al.* showed that the diffraction-limited resolution barrier may be surpassed by the simultaneous stimulated emission depletion (STED) of fluorophores to shape the point spread function (PSF) of an excitation pulse [46]. In this method two synchronized laser pulses are employed: one is an excitation pulse in the blue region of the excitation spectrum of the

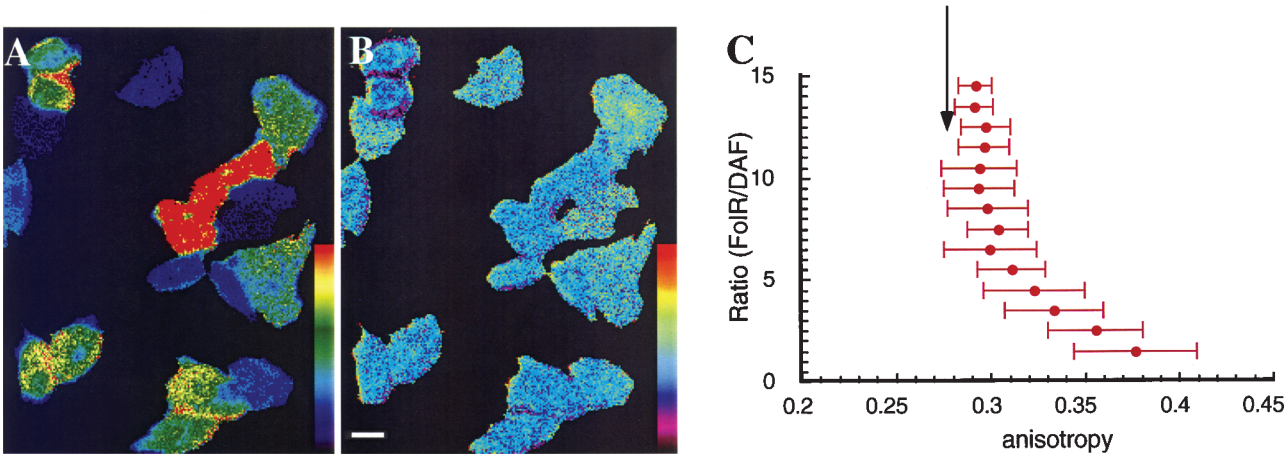

Fig. 4. Use of the D-FRET method to probe interactions between two proteins. cDNA for GPI-anchored folate receptor (FR-GPI) was transfected into CHO cells expressing variable levels of GPI-anchored decay accelerating factor (DAF). The relative ratio of expression of the DAF and FR-GPI (**A**) was determined by measuring the fluorescence intensities of Cy5-conjugated Fab fragments of monoclonal antibody IA10 against DAF and PLF, respectively. The fluorescence emission anisotropy of PLF-bound FR-GPI (**B**) was determined and images of the same were pseudo-colored and printed as described in Ref. 34. Average values of emission anisotropy of PLF-labeled FR-GPI were obtained from cells exhibiting the same relative ratio of expression of the two proteins and plotted against the indicated ratios (**C**). Note the increase in anisotropy of PLF-labeled FR-GPI with the increase in relative expression levels of DAF. These observations are consistent with the possibility that the distance between individual FR-GPI species is being increased by the presence of "interacting" DAF species. The arrow denotes the value of anisotropy of PLF-labeled FR-GPI in CHO cells expressing very low levels of other GPI-APs.

fluorophore, and the other is the STED pulse at the red edge. In the STED process, fluorophores in the outer rim of the focal spot are forced to an upper vibrational level of the ground state, and their ultrafast vibrational decay is exploited to quench the fluorescence from the rim. The time duration of the STED pulses is considerably longer (~40 ps) than that of the excitation pulse (~0.2 ps) so that the quenched molecules are deprived a chance to get reexcited by the excitation beam. The placement of a $\lambda/2$ phase plate (smaller than the beam diameter) in the path of the STED excitation laser beam ensures that the STED pulses destructively interfere at the focus and deplete the fluorophores emission only at the outer rim, thereby generating fluorescence focal spots of a substantially reduced extent and, consequently, increasing the optical resolution. Thus, the authors achieved a sixfold increase in axial resolution and a twofold increase in the lateral direction [46]. Images of live cell membranes were obtained with this method and a clear contrast was brought out with conventional confocal images. However, refractive index mismatches among the cell, the medium, and the immersion liquid of the objective reduced the extent of PSF shaping envisaged. Furthermore, there is a potential for significant photostress on the live cells as well as bleaching of fluorophores due to direct excitation of fluorophores by the STED pulse.

Diffusion Methods

The above techniques demonstrate an improvement of optical resolution by tampering with the photophysics of emission or excitation. On the other hand, diffusion characteristics of the components of the cell membrane also reveal information regarding their organization on the nanometer scale [47]. These methodologies often (but not always) employ fluorescence and imaging technology to monitor diffusing species. Fluorescence recovery after photobleaching (FRAP), single (fluorescent)-particle tracking (SPT), and fluorescence correlation spectroscopy (FCS) are examples of these methods. While these methods are beyond the scope of this review, the reader is referred to a number of reviews and publications in this area [47–50].

BIOLOGICAL APPLICATIONS

In this section, we review biological situations where different fluorescence imaging methods outlined above have been applied to probe the organization of membrane components with nanometer spatial resolution. We have restricted ourselves to recent applications that focus on imaging situations encountered in membranes of cells.

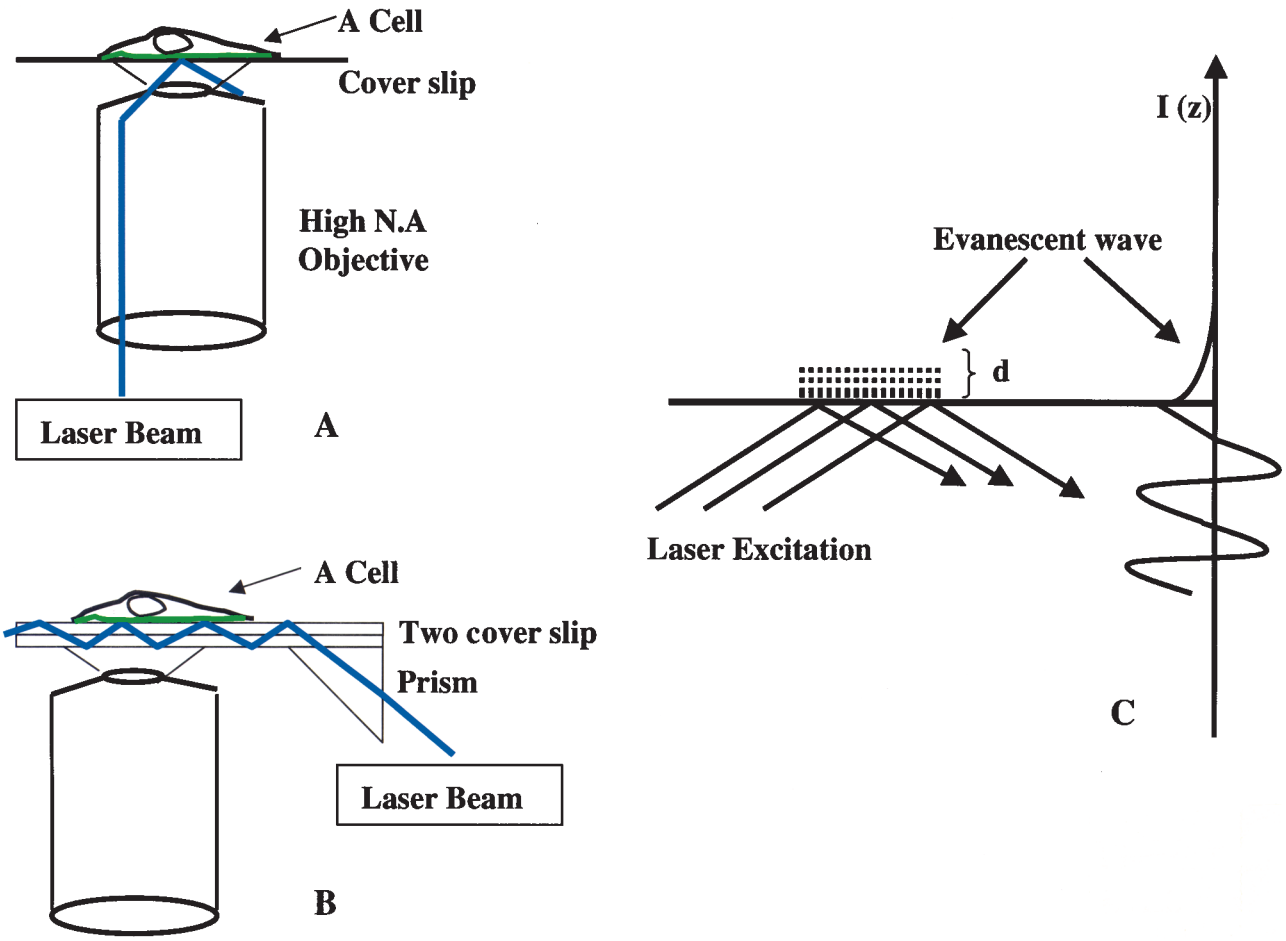

Fig. 5. Schematic of total internal reflection fluorescence microscopy (TIR-FM). (**A**) Schematic of objective-type TIR-FM. The laser beam is made to enter an objective of a high numerical aperture from the edge of the objective. (**B**) In prism-type TIR, a prism is placed at the edge of two fused coverslips with immersion oil. The laser beam entering via this prism is totally internally reflected. (**C**) Typical waveforms in a TIR phenomenon. $I(z)$ is the intensity along the z-axis, and d is the penetration depth of the evanescent wave in the aqueous medium. The green edge of the cells shows the regions of the cells which are excited by the evanescent wave.

Membrane Protein Conformation and Receptor Organization

Although the resolution obtained by X-ray diffraction methods is much higher than that obtained using FRET methods, FRET is an ideal method to study protein conformational studies of membrane proteins under physiological conditions. These methods have been extensively exploited to provide a detailed understanding of protein orientation and conformation in solution (reviewed in Refs. 29, 51, and 52).

In terms of studying subnanometer-scale conformational changes in membrane proteins, ion transport proteins have served as classic example of this type of FRET application *in vivo*. Ion transport across membranes in the case of the voltage-gated potassium channel which is made up of four homologous subunits, each of six transmembrane segments, is proposed to involve significant conformational changes in the voltage sensor segments, S4, and the S2 segments [53]. Glauner *et al.* addressed the problem of defining the structure and motion of each voltage-sensing domain by distance measurements using FRET [54]. They determined photobleaching rates of donor fluorophores in the presence and absence of acceptor fluorophores, introduced by site-specific labeling of single cysteine residues introduced at identical sites on each subunit with fluorescein (donor) or rhodamine (acceptor) maleimide. This was coupled with the measurement of photobleaching rates in the open and closed states of the channel. The change in distance observed from the FRET measurements is consistent with a twisting motion of the voltage-sensing segments during gated opening. Real-time measure-

ments of donor quenching and dequenching show that changes taking place in milliseconds are consistent with a helix that twists during channel opening. A separate study using lanthanide-based FRET detected atomic-scale (~3- to 4-Å) movements of the same voltage-sensing regions in the potassium channel [55]. This method exploited the long lifetime of the lanthanide donor fluorophore and measured donor lifetimes in the presence of an acceptor, by determining the lifetime of the sensitized emission in the microsecond region. They also measured intersubunit distances as a function of voltage, revealing that voltage-dependent movement of the subunits coincided with the gating charge movement for the same channels, thereby indicating a close correlation between the two.

Acetylcholine receptors (AChR) are ligand-gated ion channels consisting of four types of subunits assembled as a pentamer (reviewed in Ref. 56). Barrantes and coworkers have analyzed the membrane environment of the protein in AChR-rich torpedo membranes using an elegant FRET-based methodology [57]. Using the sensitized emission of an environment-sensitive lipophilic membrane probe, laurdan, by the excitation of intrinsic tryptophan donor fluorophores at 290 nm, they were able to study the properties of the membrane environment in proximity to the protein. They showed that FRET-sensitized laurdan emission detects a lipid order which differs structurally and dynamically from the bulk lipid order in terms of polarity and molecular motion. These types of studies can be easily extended to fluorescence imaging applications in living cells. Coupled with the selective introduction of fluorescent donors using site-directed mutagenesis and chemical coupling of small fluorophores *in situ* [58], these techniques have tremendous potential for exploring the organization and structure of membrane proteins.

Another level of reorganization of membrane proteins takes place upon receptor–ligand interaction. Often receptor ligation leads to a substantial change in receptor protein confirmation or subunit reorganization leading to the endocytosis of the receptor, activation of signaling cascades, and other biological consequences. Since receptor–ligand complexes usually begin as small clusters of nanometer sizes, they cannot be visualized by conventional fluorescence microscopy until they grow to relatively large clusters. The potential of FRET methods in such studies is amply demonstrated by the fact that numerous reports have used this technique as the method of choice to study protein dynamics at the cell surface ([59,60]; see also Table I in Ref. 19).

Recently, Szollosi *et al.* have reviewed the use of FRET to determine the cell surface distribution of hematopoietic clusters of differentiation molecules using flow cytometry [61]. Although flow cytometric studies provide average information from single cells, the distribution of these values has provided statistical information to infer distances between fluorescently labeled donor–acceptor pairs of Fab fragments or intact monoclonal antibodies against specific proteins. Flow cytometric FRET measurements of sensitized emission have been undertaken to investigate the topological distribution of transferrin receptor relative to the heavy and light chains of HLA class I molecules, class II molecules, and interleukin receptors (Figs. 3 and 4 in Ref. 61). A detailed flow cytometric FRET study has suggested the existence of class I HLA dimers and oligomers at the surface of live human cells in the work of Gaspar *et al.* [62]. In this study an integrated approach of computer modeling based on high-resolution structural information from X-ray crystallographic data and steric positioning from FRET-based measurements on membrane-bound HLA-I molecules in live cells has led to 3D models of supramolecular organization of class I HLA molecules under physiological conditions.

A significant advancement in understanding the specificity of interleukin receptor ligand ligation and signaling has been provided by elegant studies on the interleukin 2 (IL-2) receptor assembly by Damjanovich *et al.* [63]. The IL-2 receptor is a multisubunit receptor consisting of α, β, and γ chains. FRET measurements in terms of sensitized emission between FITC- and Cy3-conjugated monoclonal antibodies against α, β, and γ receptor subunits in pairwise combinations have revealed that the receptor subunits are already assembled as a trimer in resting T cells. However, the binding of relevant interleukins (IL-2, IL-7, and IL-15) modulates the relative organization of these subunits, providing an explanation of cytokine-specific signaling. In contrast, FRET measurements using similar FRET pairs, FITC- and Cy3-conjugated antibodies to the IL-1 receptor, suggest that the IL-1 receptor undergoes agonist (IL-1)-dependent receptor assembly essential for signal transduction; antagonists do not cause this reorganization [64].

Flow cytometric FRET analyses by sensitized acceptor emission measurements are an extremely powerful method to look at cell surface-averaged nanometer-scale interactions. This is due mainly to the possibility of obtaining statistically large numbers of cells for analysis [61]. However, spatial information at the level of the cell membrane or subcellular compartment is not available by this methodology. A combination of fluorescence imaging and FRET provides a solution to studying these interactions at least at light resolution. Bastiaens

and Jovin have employed such a strategy to study the aggregation state of the epidermal growth factor (EGF) and EGF receptor (EGFR) [33]. They have used photobleaching FRET microscopy and FLIM using fluorescein- and rhodamine-labeled EGF (as donor–acceptor pairs, respectively) bound to EGFR. These studies suggest that high-affinity EGF may in fact bind to a predimerized state of EGFR.

At even higher resolutions, Sako and co-workers [65] have utilized single-molecule fluorescence methodology to study interactions between the same receptor–ligand pair. They have used a combination of TIR–FM to detect intensity fluctuations of single molecules of Cy3-labeled EGF and the FRET pair, Cy3- and Cy5-conjugated EGF, at single-fluorophore resolution to study ligand-induced receptor dimerization. In this study they were able to observe selectively fluorescence from the basal or apical surfaces of cells attached to a substrate by varying the angle of the incident laser beam in an epiillumination arrangement (Fig. 5A) to generate the evanescent excitation. Combined fluorescence intensity measurements and FRET measurements at the single-molecule level have shown that EGF binds more efficiently to EGF–(EGFR–EGFR), consistent with the notion that EGF binding results in the dimerization of the receptor [33]. In conjunction with FRET, further studies at the single-molecule level are also likely to reveal the conformational dynamics and activity of EGFR dimers. These approaches are easily extended to other receptor ligand pairs and will be particularly useful in understanding the mechanism of receptor internalization following subunit reorganization or clustering. It will be particularly interesting to correlate nanometer-scale rearrangements of receptors with hot spots for clathrin-mediated internalization [66].

Signal Transduction

Elucidation of signaling pathways and interactions between downstream components involved in signaling cascades have only recently come under the purview of nanometer-scale resolution in living cells. Since such molecular proximities can be easily probed by FRET, measurements in living cells have revealed a variety of kinetic and spatial information regarding protein–protein interactions, enzymatic activity, and sensing of second-messenger levels. Here we describe some examples from each type of assay. Where available, examples of GFP-based FRET sensors of intracellular biochemistry are also presented (also reviewed in Refs. 67 and 68).

Once again, the interaction of EGFR with its ligand has served as a good biological model system since many of the downstream components of the EGFR signaling cascade are already known. Following receptor activation by EGF binding to EGFR, signaling is initiated through the mitogen-activated protein (MAP) kinase pathway. The first step is activation of the receptor tyrosine kinase activity followed by the interaction of EGFR with the SH2 domain of the growth factor receptor binding protein, Grb2. This in turn initiates a signaling cascade via the Ras and MAP kinase pathway. FLIM has been used to study the activity of the receptor tyrosine kinase EGFR [69], wherein phosphorylation of EGFR was monitored using FRET between GFP–EGFR and Cy3-labeled antiphosphotyrosine antibodies. In the absence of EGF stimulation, EGFR–GFP was distributed on the plasma membrane and antiphosphotyrosine immunostaining was localized to punctate structures at the cell periphery. Although GFP–EGFR was present on the plasma membrane, no FRET was observed between GFP–EGFR and Cy3-antiphosphotyrosine located in punctate structures on the plasma membrane. Upon stimulation with EGF, Cy3-antiphosphotyrosine staining colocalized with GFP–EGFR in membrane ridges and punctate endosome-like structures. Increased FRET, resulting in decreased GFP fluorescence lifetimes, was observed from these structures. There was variation in the extent of FRET measured in the various punctate structures containing phosphotyrosines, as they could represent the presence of other phosphorylated proteins. No change in GFP lifetime was observed from GFP present in the golgi and the perinuclear regions. As another control for the change in fluorescence lifetime, the authors photobleached the acceptor and showed that this resulted in uniform GFP fluorescence lifetimes across the entire cell.

Spatially resolved activation of another receptor tyrosine kinase belonging to the EGFR family, ErbB1, has also been studied by measuring GFP fluorescence lifetimes as an indicator of FRET between GFP–ErbB1 and Cy3–Fab–antiphosphotyrosine [70]. Upon EGF stimulation by EGF or EGF-coated beads in living cells expressing GFP–ErbB1, microinjected with a Cy3-labeled Fab fragment of antiphosphotyrosine antibody, there is a reduction in GFP lifetimes across the entire cell surface. The spatial distribution of the FLIM data (FRET signal) provided evidence for a new signaling mechanism involving a ligand-independent lateral propagation of receptor activation in the plasma membrane.

Interaction between Grb2 and EGFR has also been studied using FRET methodology [71]. This has allowed the visualization of spatiotemporal regulation of EGFR–Grb2 interactions on a pixel-by-pixel basis using the FRET pairs, cyan fluorescent protein (CFP) (fused to

EGFR) and yellow fluorescent protein (YFP) (fused to Grb2); YFP–Grb2 was transiently expressed in cells stably expressing CFP–EGFR. Upon EGF stimulation, EGFR–CFP and Grb2–YFP colocalized in membrane ruffles and small vesicular structures. At later times the two proteins became concentrated in large perinuclear endosome-like vesicles. FRET was measured as sensitized emission of the acceptor, YFP–Grb2. Very weak FRET was detected in unstimulated cells; the signal increased dramatically upon stimulation, especially in the membrane ruffles and early endosomes and, later, in the perinuclear region, indicating the interaction between EGFR and Grb2 upon stimulation with EGF.

In the study of a different signaling system, Devereotes *et al.* [72] have used FRET to understand signaling mechanisms of G-protein-coupled cAMP receptors in chemotacting and migrating Dictyostelium. They fused the $G\alpha_2$ subunit of the G-protein to CFP and the G_β subunit to YFP and studied the rapid association and dissociation of G-protein heterotrimers in response to the chemoattractant cAMP. CFP and YFP form a very useful energy transfer pair, and significant energy transfer was detected between CFP and YFP on unstimulated cells placed in a fluorimeter, a shoulder peak on the emission of CFP was observed which corresponded to the emission of YFP when CFP alone was excited. Upon stimulation with cAMP, this sensitized emission signal was abolished, indicating the dissociation of the two subunits which happens during signaling via G-protein-coupled receptors. The persistent activation of the G-protein cycle as measured by a reduction in the extent of FRET during times of "adaptation" to high levels of cAMP reveals a new twist to mechanisms of G-protein-coupled signal modulation. Although these observations were also confirmed using a fluorescence microscope, spatially resolved analyses remain to be performed and are likely to reveal interesting subcellular insight into the localization of G-protein signaling mechanisms.

Protein kinase C-α (PKC-α) activation in live and fixed cells has also been visualized using FLIM [73]. In an earlier approach, Bastiaens and Jovin [33] had demonstrated that purified PKC subunits may be fluorescently labeled *in vitro*, reintroduced back into cells, and their activation studied using FRET. In their recent study, they show that upon activation with tetradecanoylphorbol acetate, PKC-α is phosphorylated on threonine-250. Two antibodies, a site-specific antiserum to phosphorylated threonine-250 conjugated to Cy5 and an antibody to PKC-α (MC5) conjugated to Cy3, were used as FRET pairs to look at PKC-α activation in cells fixed postactivation. In living cells expressing GFP-tagged PKC-α, a Cy3-labeled antiserum to phosphorylated threonine-250 was microinjected. A decrease in the donor lifetime of GFP in the case of live cells and that of Cy3-MC5 in the case of fixed cells was measured. Upon activation, most of the decrease in donor lifetime, hence increased FRET, was observed from the plasma membrane and vesicular structures in the cytoplasm. PKC-α has also been implicated in integrin-mediated spreading and migration. Complexes of activated β_1-integrin and PKC-α were observed using FLIM [74]. GFP–PKC-α and Cy3-labeled 12G10 (an antibody against activated β_1-integrin) were used as FRET pairs. In unstimulated cells decreased donor lifetimes were observed in the interior of the cell with a punctate pattern of unaltered GFP lifetime at the cell periphery. Upon stimulation with TPA, increased FRET was observed between PKC-α and activated β_1-integrin all over the cells, which manifested in a further decrease in the GFP lifetime. A reduced and less frequent interaction was observed between GFP–PKC-α and nonactivated β_1-integrin.

Spatial and temporal activation of Rho-family GTPases, for example, Rac, in living cells was recently observed using a FRET-based methodology. An Alexa-546 fused biosensor termed FLAIR (fluorescence activation indicator for Rho proteins) [75] was made from p21-activated kinase 1 (PAK1), which binds specifically to Rac in its activated GTP-bound form. The p21 binding domain (PBD) was fused to Alexa-546 via an engineered cysteine and was microinjected in living cells expressing GFP–Rac. FRET was measured as the sensitized emission of the acceptor Alexa-546-labeled PBD, upon excitation of the donor GFP. Activating Swiss 3T3 fibroblasts with serum or PDGF causes them to produce membrane ruffles. Although GFP–Rac fluorescence was observed in the nucleus as well, specific Rac activation indicated by an increased FRET signal was observed only in the membrane ruffles, and not in the nucleus. This suggests that Rac is active only where there is local actin reorganization. A gradient of Rac activation is observed in migrating cells relative to the direction of movement.

A FRET-based assay for the agonist-induced phospholipase Cδ1 (PLCδ1) has been described recently [76]. In this study, the authors constructed a probe to study inositol lipid dynamics by expressing a phosphorylated inositol binding pleckstrin homology (PH) domain tagged with CFP and YFP. This donor–acceptor combination exhibits significant CFP-donor quenching due to FRET when localized to membranes. Activation of PLCδ1 with agonists of G-protein-coupled receptors causes the hydrolysis of phosphorylated inositol lipids, causing the release of the labeled PH domains into the cytosol. This increases their intermolecular sep-

aration by 200- to 1000-fold, resulting in an increase in the CFP/YFP fluorescence ratio and, thereby, serving as a reliable indicator of PLCδ1 activation.

FRET has been used to mark synaptic activity in dendritic spines [77]. A large but transient change in intracellular calcium occurs upon the induction of stable changes in synaptic strength. Calpain, a calcium-sensitive protease, is activated in neurons in response to pharmacological stimulation of glutamate receptors as well as after patterns of afferent stimulation leading to long-term potentiation (LTP). Exploiting the fact that calpain is activated in stimulated neurons, a construct was engineered which contained a μ-calpain substrate (a peptide derived from α-spectrin) sandwiched between CFP and YFP. A PDZ domain was also engineered in the construct to localize it to postsynaptic densities. By measuring the decrease in sensitized emission due to FRET, individual dendritic spines showing increased calpain activity in response to glutamatergic agonists were identified.

FRET methodology has also provided a number of sensors of important second messengers involved in signaling pathways, including Ca^{2+} and cAMP. The FRET-based sensor for calcium is referred to as "cameleon" [78,79]. It is a fusion protein consisting of CFP (or BFP) fused to calmodulin, the calmodulin-binding peptide, M13, and an enhanced GFP or YFP. Binding of calcium makes calmodulin wrap around the M13 domain, thereby increasing FRET between the two GFP molecules at the two ends. This provides the capacity to measure calcium concentrations in the 10 n*M* to 10 m*M* range with different calmodulin mutations [78]. These types of cameleons have been used to measure the concentration of calcium at the surface of secretory granules during exocytosis [80]. Recently, a similar GFP-based sensor has been engineered to detect cGMP levels in cells [81]. The role of metalothionein (MT) in nitric oxide signaling was demonstrated using a similar principle, where metalothionein was fused to two GFP moieties and metal release from it resulted in decreased FRET between the fused proteins due to a conformational change in MT [82]. Another FRET-based sensor for measuring cAMP signaling pathway consists of a cAMP-dependent protein kinase in which the catalytic (C) and regulatory (R) subunits are each labeled with a different fluorescent dye such as fluorescein or rhodamine capable of FRET. When cAMP molecules bind to the R subunits, the C subunits dissociate, thereby eliminating FRET [83]. Measurement of this dissociation by FRET provides an elegant way of monitoring local intracellular cAMP concentrations as well as the extent of kinase activation in intact cells [84,85].

These reports amply demonstrate the power of FRET techniques to resolve spatially the catalytic activity of fluorescently tagged proteins inside live cells and also to determine the functional state of proteins in fixed cells and tissues.

Lipid Microdomains or Rafts

Lipid microdomains or "rafts" enriched in cholesterol and sphingolipid have been hypothesized [86] to exist in the membrane of living cells. They have been proposed to explain the observation that many signaling and sorting properties of membrane proteins and lipids, including glycosyl phosphatidylinositol-anchored proteins (GPI-APs), are modulated by altering the cholesterol and sphingolipid levels. However, these lateral heterogenieties have been difficult to visualize by means of fluorescence microscopy and electron microscopy (reviewed in Ref. 87). The elusive nature of these rafts may be related to the lack of suitable methodology to visualize nanometer-scale organization in living cell membranes, since lipid microdomains are predicted to be submicron-sized entities [88]. To probe these domains, FRET techniques have served as a useful biophysical tool. Varma and Mayor have demonstrated the existence of a clustered organization of GPI-APs by the use of D-FRET microscopy [34]. Using this method, they measured the extent of homotransfer between GPI-anchored and transmembrane-anchored isoforms of folate receptors bound to a fluorescein-conjugated analogue of folic acid, *N*α-pteroyl-*N*ε-(4′-fluorescein-thiocarbamoyl)-L-lysine (PLF). They found that the extent of energy transfer of the GPI-anchored folate receptor isoform was independent of the fluorophore density, consistent with submicron-sized clusters at the surface of living cells. Furthermore, these clusters were sensitive to cholesterol levels in cells. In contrast, the transmembrane isoform where the anisotropy was found to be dependent on concentration was insensitive to cholesterol levels. Using this methodology it can also be shown that more than one kind of GPI-anchored protein can become part of the same cluster at the cell surface (Fig. 4).

In two separate studies, Kenworthy *et al.* [22,89] employed the acceptor photobleaching methodology to measure FRET between Cy3- and Cy5-labeled Fab fragments against different GPI-APs, including the folate receptor and 5′-nucleotidase in MDCK cells. They found that the energy transfer efficiency was correlated with the density of proteins in cells and thus inferred that these proteins were not clustered and may be randomly distributed [22]. However, it is likely that if lipid rafts

are small and only a small fraction of proteins is present in these structures [88], the FRET signal measured by acceptor photobleaching signals may be swamped out at low densities of GPI-AP expression due to a dilution effect by endogenous GPI-APs or other raft components (Edidin, 2001, www.stke.org [39] (Fig. 4). Hwang *et al.* have used NSOM to investigate the organization of BODIPY-PC-labeled plasma membranes of fixed human skin fibroblasts and they detected patchiness of the fluorescence in images which were consistent with the sizes of membrane domains estimated earlier by FRAP measurements [43].

Supportive evidence for lipid domains also comes from diffusion measurements such as FRAP, SPT (reviewed in Refs. 47 and 88) and photonic force microscopy [90]. Despite these methodologies exploiting FRET and NSOM and the large number of diffusion studies to provide evidence for the existence of lipid domains/rafts, the structure and function of these rafts in biological contexts remain an open question [91,92].

Cell Surface Topology and Dynamics

The study of the cell surface and its topology by fluorescence imaging methods is likely to benefit greatly from the application of NSOM methodology. Enderle *et al.* have described the use of NSOM to map and detect simultaneously colocalized proteins within the membrane of a fixed and air-dried malaria parasite-infected red blood cell, with a resolution greater than that of a confocal microscope [93]. Using spatial correlation, these studies revealed the association of the parasite proteins with host skeletal proteins on the red cell membrane. In another study, Subramaniam *et al.* combined imaging with both NSOM and FRET at the surface of epidermoid carcinoma cells [44]. They demonstrated the possibility of studying interactions between a receptor–ligand pair on a highly localized spatial scale (10–100 nm), coupled to the high-resolution mapping of surface topography by using a readout of the force field. Other measurements using the NSOM technique include membrane-specific mapping and accurate localization (up to 10- to 100-nm resolution) of the proteins and probing surface domains of the plasma membrane in fixed and dried human skin fibroblasts [43]. However, measurements in membranes of living cells and tissues are yet to be realized with a resolution higher than that obtained with confocal excitation [43].

In a recent study, AFM and TIR-FM have been combined for the study of force transmission in endothelial cells [94]. Variable-angle TIR-FM experiments were conducted in an inverted microscope configuration and actin filaments were stained with rhodamine–phalloidin. Elastic moduli systematically decreased from the nucleus (~7.2 kPa) toward the cell body near the surface (~1.27 kPa), suggesting that the nucleus is stiffer than the rest of the cell body. An AFM tip was used to produce local stress (0.3–0.5 nN) in the apical surface and TIR-FM was employed to excite fluorescence in the basal membrane of the cells. Apparently, there seem to be global focal contact rearrangements in response to these local applied forces. Significant changes occurred in cell–substrate contacts in position and focal contact distribution when these localized forces were removed. This study, although carried out in fixed cells, demonstrates the pattern of force transmission from the apical surface to the basal surface in an adherent cell system, although it could not show the direct contribution of the cytoskeleton in such force transmission [94]. Another demonstration of multiple-angle TIR-FM is in mapping fluorophore distributions in 3D in living cells by obtaining images at multiple incident angles [95]. Theoretical analysis was developed in this study to compute the fluorophore *z*-distribution by inverse Laplace transform of angle-resolved intensity functions. The potential of probing at nanometer resolution at the cell–substrate contact regions was shown for fibroblasts and epithelial cells.

An important attribute of TIR-FM, as in any other quantitative fluorescence imaging method, is that the steady-state fluorescence is proportional to the surface density of molecules. Thus, information regarding the real-time dynamics of surface fluorophore distribution may be obtained with an extremely high *z*-resolution. In two separate studies, Schmoranzer *et al.* and Toomre *et al.*, respectively, have utilized this property to image the final stages of constitutive exocytosis of a GFP-tagged membrane protein, VSV-G, at a high axial resolution (~70 nm) and a good temporal resolution (30 frames/s) using objective-based TIR-FM [96] or prism-based TIR-FM illumination, conditions which gave similar results [97]. Using TIR-FM, investigators have also been able to study the delivery of exocytic vesicles to the plasma membrane, to record the final stages of vesicle fusion with the plasma membrane [98], and to study the motion of cortical secretory granules in chromaffin cells [99].

In summary, we have surveyed a range of microscopic methods available for imaging phenomena in biological systems with nanometer resolution. These techniques are likely to unravel valuable information regarding the organization and dynamics of molecules in membranes, leading to insights into biological function.

FUTURE PERSPECTIVES

As the number of applications of conventional FRET microscopy continues to increase, there is a parallel development of novel fluorescent probes to enhance the applicability and reliability of these methodologies. This includes modifications in genetically encoded dyes, such as GFP and its mutants [6,67,78,100], as well as nongenetically encoded probes [58]. A significant development in FRET donor dyes is the use of lanthanide atoms, which offer the ability to measure distances as large as 10 nm and with a greater accuracy in measurements [28,30,55,101]. For example, lanthanide-based FRET has been used to measure relatively long distances (7–8 nm) in myosin [101]. The concurrent development of novel dyes and new imaging methodologies certainly bodes well for the possibility of imaging on the nanometer scale in living cells. The ability to locate fluorophores at specific sites in proteins by site-directed mutagenesis to incorporate noncanonical amino acids [102] or tetracysteine domains, coupled with the ability to label these sites *in vivo* [58], will certainly aid in understanding membrane protein structure and dynamics at nanometer resolution.

All improvements in conventional fluorescence microscopy have focused on a single theme of enhancing the spatial/temporal resolution in visualization of processes in living cells. The recent possibility of fluorescence microscopy with significantly enhanced resolution, using STED combined with TIR-FM to create spatially controlled excitation profiles [46], is a promising development. In addition to FRET measurements on an ensemble of molecules, applications of FRET on a single-molecule scale are finding their niche in combination with TIR-FM and NSOM excitation strategies [65,103]. Along with the ability to make diffusion measurements in living cells, the potential of single-molecule imaging in living cells is heralding a new era in cellular biology. An important reason for this is the advancement in the technology of detection of fluorophores and advanced imaging systems. Extremely sensitive, low-light detectors and sophisticated image processing techniques are revolutionizing the field of fluorescence microscopy to put it in a rigorous quantitative framework as opposed to its being a mere visualization tool. This has also allowed cellular systems and processes to be subjected to sophisticated theoretical modeling.

ACKNOWLEDGMENTS

We would like to thank Pranav Sharma for sharing his unpublished observations, M. K. Mathew for critically reading the manuscript, and A. Chattopadhyay for his patience. S.M. is a Senior Research Fellow of The Wellcome Trust and is grateful to K. Belur and F. F. Bosphorus for providing inspiration.

REFERENCES

1. W. Baumeister, R. Grimm, and J. Walz (1999) *Trends Cell Biol.* **9**, 81–85.
2. J. B. Pawley (1995). *Handbook of Biological Confocal Microscopy*, Plenum Press, New York.
3. D. L. Taylor, and Y. Wang (1989) *Fluorescence Microscopy of Living Cells (Part A)*, Academic Press, San Diego.
4. R. P. Haugland (1996) *Handbook of Fluorescent Probes and Research Chemicals*, Molecular Probes, Eugene, OR.
5. R. Y. Tsien and A. Waggoner (1995) in J. B. Pawley (Ed.), *Handbook of Biological Confocal Microscopy*, Plenum Press, New York, pp. 267–279.
6. J. Ellenberg, J. Lippincott-Schwartz, and J. F. Presley, (1999) *Trends Cell Biol.* **9**, 52–56.
7. V. T. Oi, A. N. Glazer, and L. Stryer (1982) *J Cell Biol.* **93**, 981–986.
8. S. Maiti, J. B. Shear, R. M. Williams, W. R. Zipfel, and W. W. Webb (1997) *Science* **275**, 530–532.
9. S. Inoue (1986) *Video Microscopy*, Plenum Press, New York.
10. B. Herman (1989) in *Fluorescence Microscopy of Living Cells in Culture (Part B)*, San Diego, Vol. 30, pp. 220–243.
11. K. Lieberman, S. Harush, A. Lewis, and R. Kopelman (1990) *Science* **247**, 59–61.
12. A. Lewis, A. Radko, N. Ben Ami, D. Palanker, and K. Lieberman (1999) *Trends Cell Biol.* **9**, 70–73.
13. L. K. Tamm (1993) in B. Herman and J. J. Lemasters (Eds.), *Optical Microscopy: Emerging Methods and Application*, Academic Press, San Diego, pp. 295–337.
14. D. Axelrod (1989) in D. L. Taylor and Y. Wang (Eds.), *Fluorescence Microscopy of Living Cells in Culture (Part B)*, Academic Press, San Diego, Vol. 30, pp. 245–270.
15. L. Stryer (1978) *Annu. Rev. Biochem.* **47**, 819–846.
16. R. E. Dale, J. Eisinger, and W. E. Blumberg (1979) *Biophys. J.* **26**, 161–193.
17. P. Wu and L. Brand (1992) *Biochemistry* **31**, 7939–7947.
18. C. G. dos Remedios and P. D. Moens (1995) *J. Struct. Biol.* **115**, 175–185.
19. T. M. Jovin and D. J. Arndt-Jovin (1989) in E. Kohen and J. G. Hirschberg (Eds.), *Cell Structure and Function by Microspectrofluorometry*, Academic Press, San Diego, pp. 99–117.
20. K. W. Dunn, S. Mayor, J. N. Myers, and F. R. Maxfield (1994) *FASEB J.* **8**, 573–582.
21. G. R. Bright, G. W. Fisher, J. Rogowska, and D. L. Taylor (1989) in D. L. Taylor and Y. Wang (Eds.), *Fluorescence Microscopy of Living Cells in Culture (Part B)*, Academic Press, San Diego, Vol. 30, pp. 157–192.
22. A. K. Kenworthy and M. Edidin (1998) *J. Cell Biol.* **142**, 69–84.
23. A. K. Kenworthy and M. Edidin (1999) in M. H. Gelb (Ed.), *Protein Lipidation Protocols*, Humana Press, Totowa, NJ, pp. 37–49.
24. J. Matko and M. Edidin (1997) *Methods Enzymol.* **278**, 444–462.
25. G. W. Gordon, G. Berry, X. H. Liang, B. Levine, and B. Herman (1998) *Biophys. J.* **74**, 2702–2713.
26. P. Nagy, G. Vamosi, A. Bodnar, S. J. Lockett, and J. Szollosi (1998) *Eur. Biophys. J.* **27**, 377–389.
27. N. Billinton and A. W. Knight (2001) *Anal. Biochem.* **291**, 175–197.
28. P. R. Selvin and J. E. Hearst (1994) *Proc. Natl. Acad. Sci. USA* **91**, 10024–10028.
29. P. R. Selvin (2000) *Nat. Struct. Biol.* **7**, 730–734.

30. G. Vereb, E. Jares-Erijman, P. R. Selvin, and T. M. Jovin (1998) *Biophys. J.* **74**, 2210–2222.
31. T. Oida, Y. Sako, and A. Kusumi (1993) *Biophys. J.* **64**, 676–685.
32. P. I. Bastiaens and A. Squire (1999) *Trends Cell Biol.* **9**, 48–52.
33. P. I. Bastiaens and T. M. Jovin (1996) *Proc. Natl. Acad. Sci. USA* **93**, 8407–8412.
34. R. Varma and S. Mayor (1998) *Nature* **394**, 798–801.
35. G. Weber (1954) *Trans. Faraday Soc.* **50**, 552–555.
36. J. R. Lakowicz (1999) *Principles of Fluorescence Spectroscopy,* Plenum Press, New York.
37. V. M. Agranovich and M. D. Galanin (1982) *Electronic Excitation Energy Transfer in Condensed Matter,* North-Holland, Amsterdam.
38. L. W. Runnels and S. F. Scarlata (1995) *Biophys. J.* **69**, 1569–1583.
39. P. Sharma, R. Varma, and S. Mayor (2000) *Mol. Biol. Cell* **11**, 316a.
40. I. Gautier, M. Tramier, C. Durieux, J. Coppey, R. B. Pansu, J. C. Nicolas, K. Kemnitz, and M. Coppey-Moisan (2001) *Biophys. J.* **80**, 3000–3008.
41. A. Volkmer, V. Subramaniam, D. J. Birch, and T. M. Jovin (2000) *Biophys. J.* **78**, 1589–1598.
42. S. E. Sund, J. A. Swanson, and D. Axelrod (1999) *Biophys. J.* **77**, 2266–2283.
43. J. Hwang, L. A. Gheber, L. Margolis, and M. Edidin (1998) *Biophys. J.* **74**, 2184–2190.
44. V. Subramaniam, A. K. Kirsch, and T. M. Jovin (1998) *Cell. Mol. Biol. (Noisy-le-grand)* **44**, 689–700.
45. S. Nie and R. N. Zare (1997) *Annu. Rev. Biophys. Biomol. Struct.* **26**, 567–596.
46. T. A. Klar, S. Jakobs, M. Dyba, A. Egner, and S. W. Hell (2000) *Proc. Natl. Acad. Sci. USA* **97**, 8206–8210.
47. M. J. Saxton and K. Jacobson (1997) *Annu. Rev. Biophys. Biomol. Struct.* **26**, 373–399.
48. S. Maiti, U. Haupts, and W. W. Webb (1997) *Proc. Natl. Acad. Sci. USA* **94**, 11753–11757.
49. E. L. Elson and H. Quian (1989) in D. L. Taylor and Y. Wang (Eds.), *Fluorescence Microscopy of Living Cells in Culture (Part B),* Academic Press, Vol. 30, pp. 307–332.
50. D. Wolf (1989) in D. L. Taylor and Y. Wang (Eds.), *Fluorescence Microscopy of Living Cells in Culture (Part B),* San Diego, Vol. 30, pp. 271–306.
51. M. K. Mathew (1997) *J. Indian Soc. Radiat. Photochem. Sci.* **8**, 20–25.
52. S. Weiss (2000) *Nat. Struct. Biol.* **7**, 724–729.
53. J. M. Gulbis, M. Zhou, S. Mann, and R. MacKinnon (2000) *Science* **289**, 123–127.
54. K. S. Glauner, L. M. Mannuzzu, C. S. Gandhi, and E. Y. Isacoff (1999) *Nature* **402**, 813–817.
55. A. Cha, G. E. Snyder, P. R. Selvin, and F. Bezanilla (1999) *Nature* **402**, 809–813.
56. F. J. Barrantes (1998) *The Nicotinic Acetylcholine Receptor,* Springer Verlag, Berlin.
57. S. S. Antollini, M. A. Soto, I. Bonini de Romanelli, C. Gutierrez-Merino, P. Sotomayor, and F. J. Barrantes (1996) *Biophys. J.* **70**, 1275–1284.
58. B. A. Griffin, S. R. Adams, and R. Y. Tsien (1998) *Science* **281**, 269–272.
59. B. Catipovic, G. Talluri, J. Oh, T. Wei, X. M. Su, T. E. Johansen, M. Edidin, and J. P. Schneck (1994) *J. Exp. Med.* **180**, 1753–1761.
60. A. L. Kindzelskii, M. M. Eszes, R. F. Todd, 3rd, and H. R. Petty (1997) *Biophys. J.* **73**, 1777–1784.
61. J. Szollosi, S. Damjanovich, and L. Matyus (1998) *Cytometry* **34**, 159–179.
62. R. Gaspar, Jr., P. Bagossi, L. Bene, J. Matko, J. Szollosi, J. Tozser, L. Fesus, T. A. Waldmann, and S. Damjanovich (2001) *J. Immunol.* **166**, 5078–5086.
63. S. Damjanovich, L. Bene, J. Matko, A. Alileche, C. K. Goldman, S. Sharrow, and T. A. Waldmann (1997) *Proc. Natl. Acad. Sci. USA* **94**, 13134–13139.
64. C. Guo, S. K. Dower, D. Holowka, and B. Baird (1995) *J. Biol. Chem.* **270**, 27562–27568.
65. Y. Sako, S. Minoghchi, and T. Yanagida (2000) *Nat. Cell Biol.* **2**, 168–172.
66. I. Gaidarov, F. Santini, R. A. Warren, and J. H. Keen (1999) *Nat. Cell Biol.* **1**, 1–7.
67. B. A. Pollok and R. Heim (1999) *Trends Cell Biol.* **9**, 57–60.
68. F. S. Wouters, P. J. Verveer, and P. I. Bastiaens (2001) *Trends Cell. Biol.* **11**, 203–211.
69. F. S. Wouters and P. I. Bastiaens (1999) *Curr. Biol.* **9**, 1127–1130.
70. P. J. Verveer, F. S. Wouters, A. R. Reynolds, and P. I. Bastiaens (2000) *Science* **290**, 1567–1570.
71. A. Sorkin, M. McClure, F. Huang, and R. Carter (2000) *Curr. Biol.* **10**, 1395–1398.
72. C. Janetopoulos, T. Jin, and P. Devreotes (2001) *Science* **291**, 2408–2411.
73. T. Ng, D. Shima, A. Squire, P. I. Bastiaens, S. Gschmeissner, M. J. Humphries, and P. J. Parker (1999) *Embo J* **18**, 3909–3923.
74. T. Ng, A. Squire, G. Hansra, F. Bornancin, C. Prevostel, A. Hanby, W. Harris, D. Barnes, S. Schmidt, H. Mellor, P. I. Bastiaens, and P. J. Parker (1999) *Science* **283**, 2085–2089.
75. V. S. Kraynov, C. Chamberlain, G. M. Bokoch, M. A. Schwartz, S. Slabaugh, and K. M. Hahn (2000) *Science* **290**, 333–337.
76. J. van Der Wal, R. Habets, P. Varnai, T. Balla, and K. Jalink (2001) *J. Biol. Chem.* **276**, 15337–15344.
77. P. W. Vanderklish, L. A. Krushel, B. H. Holst, J. A. Gally, K. L. Crossin, and G. M. Edelman (2000) *Proc. Natl. Acad. Sci. USA* **97**, 2253–2258.
78. A. Miyawaki, J. Llopis, R. Heim, J. M. McCaffery, J. A. Adams, M. Ikura, and R. Y. Tsien (1997) *Nature* **388**, 882–887.
79. A. Miyawaki, O. Griesbeck, R. Heim, and R. Y. Tsien (1999) *Proc. Natl. Acad. Sci. USA* **96**, 2135–2140.
80. E. Emmanouilidou, A. G. Teschemacher, A. E. Pouli, L. I. Nicholls, E. P. Seward, and G. A. Rutter (1999) *Curr. Biol.* **9**, 915–918.
81. A. Honda, S. R. Adams, C. L. Sawyer, V. V. Lev-Ram, R. Y. Tsien, and W. R. Dostmann (2001) *Proc. Natl. Acad. Sci. USA* **98**, 2437–2442.
82. L. L. Pearce, R. E. Gandley, W. Han, K. Wasserloos, M. Stitt, A. J. Kanai, M. K. McLaughlin, B. R. Pitt, and E. S. Levitan (2000) *Proc. Natl. Acad. Sci. USA* **97**, 477–482.
83. S. R. Adams, A. T. Harootunian, Y. J. Buechler, S. S. Taylor, and R. Y. Tsien (1991) *Nature* **349**, 694–697.
84. W. A. Sather, T. Tanabe, J. F. Zhang, Y. Mori, M. E. Adams, and R. W. Tsien (1993) *Neuron* **11**, 291–303.
85. B. J. Bacskai, B. Hochner, M. Mahaut-Smith, S. R. Adams, B. K. Kaang, E. R. Kandel, and R. Y. Tsien (1993) *Science* **260**, 222–226.
86. K. Simons and E. Ikonen (1997) *Nature* **387**, 569–570.
87. F. R. Maxfield and S. Mayor (1997) in F. Haag and F. Koch-Nolte (Eds.), *ADP-Ribosylation in Animal Tissues: Structure Function and Biology of Mono(ADP-Ribosyl) Transferases and Related Enzymes*, Plenum Press, New York, Vol. 419, pp. 355–364.
88. K. Jacobson and C. Dietrich (1999) *Trends Cell Biol.* **9**, 87–91.
89. A. K. Kenworthy, N. Petranova, and M. Edidin (2000) *Mol. Biol. Cell* **11**, 1645–1655.
90. A. Pralle, P. Keller, E. L. Florin, K. Simons, and J. K. Horber (2000) *J. Cell Biol.* **148**, 997–1008.
91. S. Mayor (2000) in N. Young (Ed.), *Paraxosymal Nocturnal Hemoglobinaria and the GPI-Linked Proteins*, Academic Press, New York, pp. 221–238.
92. S. Mayor and T. V. Kurzchalia (1999) in A. Hoessli and Y. Ilangumaran (Eds.), *GPI-Anchored Membrane Proteins and Carbohydrates*, R. G. Landes, Austin, TX, p. 215.
93. T. Enderle, T. Ha, D. F. Ogletree, D. S. Chemla, C. Magowan, and S. Weiss (1997) *Proc. Natl. Acad. Sci. USA* **94**, 520–525.

94. A. B. Mathur, G. A. Truskey, and W. M. Reichert (2000) *Biophys. J.* **78**, 1725–1735.
95. B. P. Olveczky, N. Periasamy, and A. S. Verkman (1997) *Biophys. J.* **73**, 2836–2847.
96. J. Schmoranzer, M. Goulian, D. Axelrod, and S. M. Simon (2000) *J. Cell Biol.* **149**, 23–32.
97. D. Toomre, J. A. Steyer, P. Keller, W. Almers, and K. Simons (2000) *J. Cell Biol.* **149**, 33–40.
98. M. Oheim, D. Loerke, W. Stuhmer, and R. H. Chow (1998) *Eur. Biophys. J.* **27**, 83–98.
99. L. M. Johns, E. S. Levitan, E. A. Shelden, R. W. Holz, and D. Axelrod (2001) *J. Cell Biol.* **153**, 177–190.
100. H. Mizuno, A. Sawano, P. Eli, H. Hama, and A. Miyawaki (2001) *Biochemistry* **40**, 2502–2510.
101. M. Xiao, H. Li, G. E. Snyder, R. Cooke, R. G. Yount, and P. R. Selvin (1998) *Proc. Natl. Acad. Sci. USA* **95**, 15309–15314.
102. D. V. Mendel, V. W. Cornish, and P. G. Schultz (1995) *Annu. Rev. Biophys. Biomol. Struct.* **24**, 435–462.
103. S. A. Vickery and R. C. Dunn (1999) *Biophys. J.* **76**, 1812–1818.